ISSN Number: 2454-2024(Online)

International Journal of Technical Research & Science

DEVELOPMENT OF INTELLIGENT CONTROL STRATEGY ON MULTILEVEL INVERTER FOR PMSG BASED WIND ENERGY CONVERSION SYSTEM

Rohan Pratap Singh, Deepak Kumar Joshi, Nirma Kumari Sharma
E-Mail Id: rps.pratapsingh96@gmail.com
Department of Electrical Engineering, Mewar University, Chittorgarh, Rajasthan, India

Abstract-The limitations of fossil fuel-based energy sources, such as rising prices, environmental harm, scarcity, and pollution, underscore the urgency of transitioning to renewable energy. Harnessing wind energy efficiently requires implementing various control strategies due to its unpredictable nature. This paper introduces a 3L multilevel converter integrated with a Permanent Magnet Synchronous Generator (PMSG)-based wind energy conversion system (WECS). It delves into the design considerations of WECS components, encompassing the fundamental models of two drivetrains and wind turbines. The adaptive fuzzy logic control, coupled with a PI type maximum power point tracking (MPPT) algorithm, optimizes wind energy extraction. Additionally, the utilization of 3-L multilevel converters enhances the system's efficiency. The primary objective is to maximize energy extraction from the wind, ensuring the system's high efficiency. To achieve maximum power point tracking across diverse conditions, the developed control algorithm undergoes rigorous testing using simulation software. By integrating diode rectifiers, 3-L boost converters, and 3-L multilevel inverters, the system maintains balanced and regulated output voltage, current, and power amidst varying input/output conditions and disturbances. Compared to conventional methods, the Intelligent Control Strategy proves superior, exhibiting enhanced stability, precision, and performance with robust dynamic response under fluctuating wind speeds.

Keywords: PMSG, WECS, MLC, FLC, NPC, DC to DC boost converter.

1. INTRODUCTION

The study about various important aspects of renewable resource, global market shares of wind turbine manufacturers, various states generated power scenarios in India, future planning of these power resources, wind power system and their status in India and global. There are two types of energy sources in the world renewable energy source and conventional energy sources. Renewable energy sources are the type of energy sources which are plenty in quantity and are derived from earth. Wind energy, solar energy, geo thermal and bio mass are different types of renewable energy sources. These resources are inexhaustible in nature. The known advantages of renewable energy sources are its clean nature, abundant in quantity and most importantly it is ecofriendly unlike non renewable energy sources. Now days more research is going on the enhancement of technology which can efficiently convert these renewable energy sources into useful electrical energy sources. Though the literal conversion efficiency of renewable energy sources is lower than that of conventional energy source, the technology is developed and improvised on daily basis to improve its efficiency above 90%. The price of electricity generation by wind power plant is comparatively lesser than other modes of generation. In a year many large utility scale wind power plants are installed. There are different components of a wind energy conversion system (WECS), of which the most important is the type of generator used. There are several types of generators used such as self-excited induction generator (SEIG), doubly fed Induction generator (DFIG), permanent magnet synchronous generator (PMSG).

2. WIND TURBINE DYNAMIC MODEL

Below are the expressions defining the wind turbine Characteristics. Wind power,

$$P_{wind} = \frac{1}{2}\rho A v^3 C_p(\lambda, \theta) \quad (1)$$

Here ρ = air density(kg/m^3)
A = rotor blades cross sectional area (m^2)
V = wind speed (m/s)
C_p = Rotor efficiency or power coefficient = function of TRS & pitch angle ( ).

At particular TSR C_p obtained is at peak. It depends on the turbine aerodynamic design. The rotor speed must be matched with wind speed (high for and low for low) so as to keep TSR fixed. For functioning high TSR wind turbines are taken rather than wind speeds with large span.

By measurement a non linear group of C_p – curves is obtained which has main consideration as pitch angle.

$$C_p = C_1(C_2 - C_3\theta - C_4)\exp(-C_5) \quad (2)$$

Proper adjustment of $C_1 – C_5$ gives good simulation results for given turbine. In this study, Table 1 gives values for $C_1 – C_5$. Fig. 1 shows the characteristic curves of $C_{p\text{-}\lambda}$ for different pitch angles. We can observe from various curves in Fig. when the pitch angle is 2 degrees, then ratio of tip speed has large values & the peak value of C_p is

0.35, which is appropriate for manufacturing of wind turbines to work for different values of wind speeds. As the pitch angle increases the value of tip speed ratio& maximum value of power coefficient reduces significantly.

Table-2.1 Various Values of C1 – C5

C_1	0.5
C_2	116/k□
C_3	0.4
C_4	5
C_5	21/k□

In above table 1 purpose of k□ □is to calculate C_2 & C_5 & it can be find out using λ & □:

$$k_\theta = \left[\frac{1}{\lambda + 0.08\theta} - \frac{0.035}{\theta^3 + 1}\right]^{-1} \quad (3)$$

PMSG doesn't have gearbox. Its power density is high and is small in size. Also, needs external excitation. All these points make it a favorable for WECS.

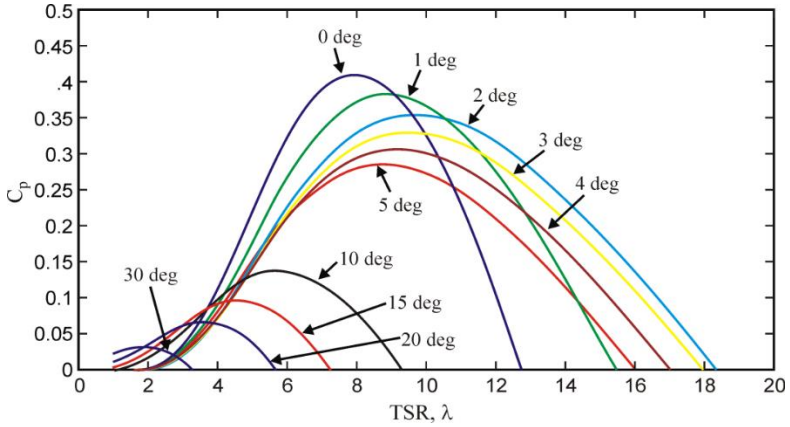

Fig. 2.1 Characteristics of C_p-λ at Various Pitch Angles (□)

While modeling PMSG back e.m.f. (sinusoidal) is considered. There is no saturation and it has only minor iron losses. PMSG dynamic currents equations,

$$\frac{di_{md}}{dt} = \frac{1}{L_d}(v_d - R_{st}i_d + \omega L_q i_{mq}), \quad (4)$$

$$\frac{di_{mq}}{dt} = \frac{1}{L_d}(v_q - R_{st}i_q + \omega L_q i_{md} - \omega\psi_{PM}), \quad (5)$$

$$i_d = \frac{1}{R_c}(L_d\frac{di_{md}}{dt} - \omega L_q i_{mq} + R_c i_{md}), \quad (6)$$

$$i_q = \frac{1}{R_c}(L_q\frac{di_{mq}}{dt} + \omega L_d i_{md} + \omega\psi_{PM} + R_c i_{mq}), \quad (7)$$

$$i_{cd} = i_d - i_{md}, \quad (8)$$

$$i_{cq} = i_q - i_{mq}, \quad (9)$$

i_q & i_d, = d_q axes currents, V_q & V_d,= d_q axes voltages, i_{cd}' i_{cq} = d_q axes iron losses currents, i_{md}, i_{mq} = d_q axes magnetizing currents, L_d, L_q=d_q axis inductances, Ψ_{pm} i=mutual flux of magnets, ω = stator currents fundamental frequency, R_c = iron losses resistance & R_{st} = stator resistance PMSG electromagnetic torque.

$$T_e = \frac{2}{3}p\left[\psi_{PM}i_{mq} + (L_d - L_q)i_{md}i_{mq}\right] \quad (10)$$

p = number of pole pairs

2.2 Two Mass Drive Train

For generating small power there are two generators

- Self-excited induction generator and PMSG

RPM of wind turbine and rotor is low and high respectively. Gearbox gives the generator turbine required speed by converting wind turbine low speed. Gearbox is not need in multi pole machines. Two mass drive train is expressed as,

$$2H\frac{d\omega_t}{dt} = T_m - T_s$$

$$T_s = K_{SS}\theta_{sta} + D_t\frac{d\theta_{sta}}{dt} \quad (3.11)$$

Where is the inertia constant of the triangle, θ_{sta} is the shaft twist angle, $\omega_t$is the angular speed of the wind turbine, ω_r is the rotor speed of the generator, ω_{ebs} is the electrical base speed, T_s is the shaft torque, is K_{ss} the Shaft stiffness, D_t is the Damping coefficients. Fig. 2.

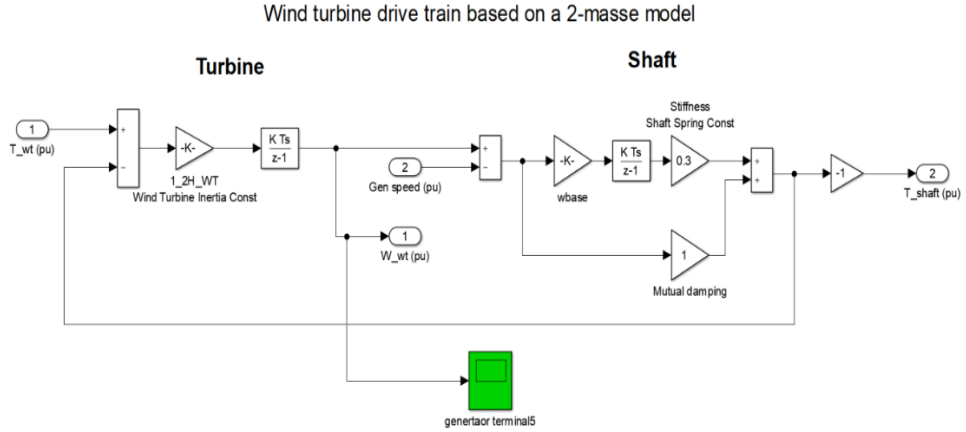

Fig. 2.2 Simulink Model of Two Mass Drive Train for Wind Turbine

2.3 Modeling of PMSG

The circuit diagram of the machine performing as a generator is shown in Fig. 2.3. The dynamic equation associated to the generating mode of maneuver is mathematically given as

$$V_t = E_r - I_a(R_a + jX_L) \quad (11)$$

Where Ra is the machine resistance, X_L is leakage reactance in series with the resistance amid the terminal voltage and air gap e.m.f. for each machine phase

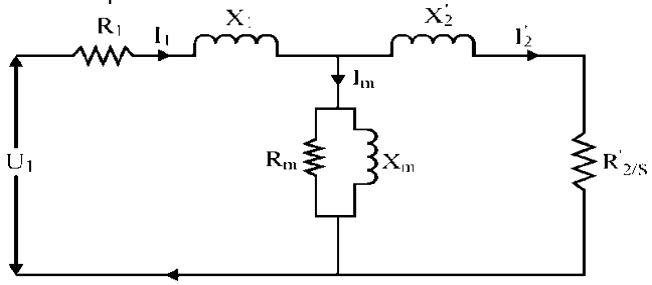

Fig. 2.3 Circuit diagram of PMSG

The PMSG model is presented in Fig. 2.3. This dynamic model assumes no dissemination, a sinusoidal back e.m.f. and insignificant eddy current and hysteresis losses. It takes into account the iron losses and the dynamic equations for the PMSG currents are:

$$\frac{di_{md}}{dt} = \frac{1}{L_d}(v_d - R_{st}i_d + \omega L_q i_{mq}), \quad (12)$$

$$\frac{di_{mq}}{dt} = \frac{1}{L_d}(v_q - R_{st}i_q + \omega L_q i_{md} - \omega\psi_{PM}), \quad (13)$$

$$i_d = \frac{1}{R_c}(L_d\frac{di_{md}}{dt} - \omega L_q i_{mq} + R_c i_{md}), \quad (14)$$

$$i_q = \frac{1}{R_c}(L_q\frac{di_{mq}}{dt} + \omega L_d i_{md} + \omega\psi_{PM} + R_c i_{mq}), \quad (15)$$

$$i_{cd} = i_d - i_{md}, \quad (16)$$

$$i_{cq} = i_q - i_{mq}, \quad (17)$$

where id, i_q are the d_q axes currents, V_d, V_q are the d_q axes voltages, i_{cd}, i_{cq} are the d_q axes iron losses currents, i_{md}, i_{mq} are the d_q axes magnetizing currents, L_d, L_q are the d_q axes inductances, If ψ_{PM} is the mutual flux due to magnets, R_c is the iron losses resistance and R_{st} is the stator resistance.
The electromagnetic torque equation of the PMSG is:

$$T_e = \frac{2}{3} p\left[\psi_{PM} i_{mq} + (L_d - L_q) i_{md} i_{mq}\right] \quad (18)$$

where p is the number of pole pairs.

3. DC/AC INVERTER

To convert dc power into ac power a three phase six switch DC to AC pulse width modulation VSI is used, a 3 phase VSI is linked to the utility grid or AC bus via coupling inductors & LC filters.
WECS is coupled with utility grid that is maintained at 25-kV via three-phase, 12 pulse converter. For converting dc voltage into ac voltage Inverter is used. Inverter must supply higher than utility grid to reassure power flow in the direction of grid only. WECS required more attention from the synchronization point of view. PWM approaches are used for switching of the semiconductor switches. Several techniques are available to control voltage and current of inverter. Among all available controllers most commonly used controller is PI controller.
It is necessary that the voltage-frequency of inverter must match the grid so to connect the plant to it. For this PLL is used. Using Park's transformation 3-Φ voltage-current is transformed to dq0 frame (rotating) and this is done. PI controller can easily controls the DC quantities obtained after transformation.

$$\begin{bmatrix} U_d \\ U_q \\ U_0 \end{bmatrix} = \frac{2}{3} \begin{bmatrix} \cos wt & \cos(wt - {}^{2\pi}/_{3}) & \cos(wt - {}^{2\pi}/_{3}) \\ -\sin wt & -\sin(wt - {}^{2\pi}/_{3}) & -\sin(wt - {}^{2\pi}/_{3}) \\ \frac{1}{2} & \frac{1}{2} & \frac{1}{2} \end{bmatrix} \begin{bmatrix} U_a \\ U_b \\ U_c \end{bmatrix} \quad (19)$$

The voltage-current of grid are not controllable but I_q and I_d it is feasible. Controller used for inverter voltage-current is in fig. 4.

$$e_d = I_{d\_ref} - I_d \quad (20)$$

Similarly the output of another controller is

$$e_q = I_{q\_ref} - I_q \quad (21)$$

PI regulator process e_d and e_q r. Its constant are selected such as

$$K_p = {}^{L}/_{\tau_i} \quad (22)$$

$$K_i = {}^{R}/_{\tau_i} \quad (23)$$

L & R = distribution system inductance &resistance. τ_i = current control loop time constant. PLL is a feedback system with PI regulator for utility grid phase angle tracking.

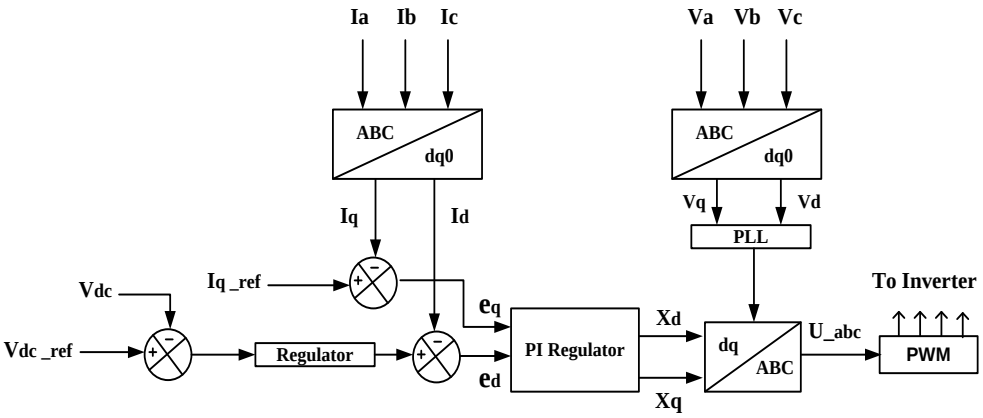

Fig. 3.1 Current Controller of Inverter with PLL

4. SIMULATION RESULT FOR MULTILEVEL INVERTER FOR PMSG BASED WIND ENERGY CONVERSION SYSTEM

Case-1: Simulation results during step-changes wind speed from 6-8-10-12 m/s

The simulation depicts a fluctuation in wind speed from 6 m/s to 8 m/s, then to 10 m/s, and finally to 12 m/s for a PMSG-based WECS with two drivetrains, while maintaining a constant load. Fig. 4.1 illustrates the simulation results. At t=0 sec., the wind speed is 8 m/s, and at t=5 sec., it reaches 12 m/s, remaining constant between these times. Notably, the wind speed transitions from 6 m/s to 8 m/s at t=1.3 sec., undergoes a step change from 8 m/s to 10 m/s at t=2.5 sec., and further steps up from 10 m/s to 12 m/s at t=3.8 sec. At t=5 sec., the PMSG output power reaches 4100W.

Fig. 4.1 illustrates that the PMSG speed decreases from 1400 rpm at t=0 to 1200 rpm at t=5 sec. Additionally, the electromagnetic torque fluctuates from 60N-m to 32N-m, and the generated power varies from 6200W to 4100W during the interval t=0 sec to t=5 sec. The generated voltage maintains regulation at 550V, and the current remains sinusoidal at 12 A, as shown in Fig. 4.1. The waveform analysis reveals that the PMSG system exhibits superior dynamic performance in response to changing wind speeds, with notable improvements in torque response.

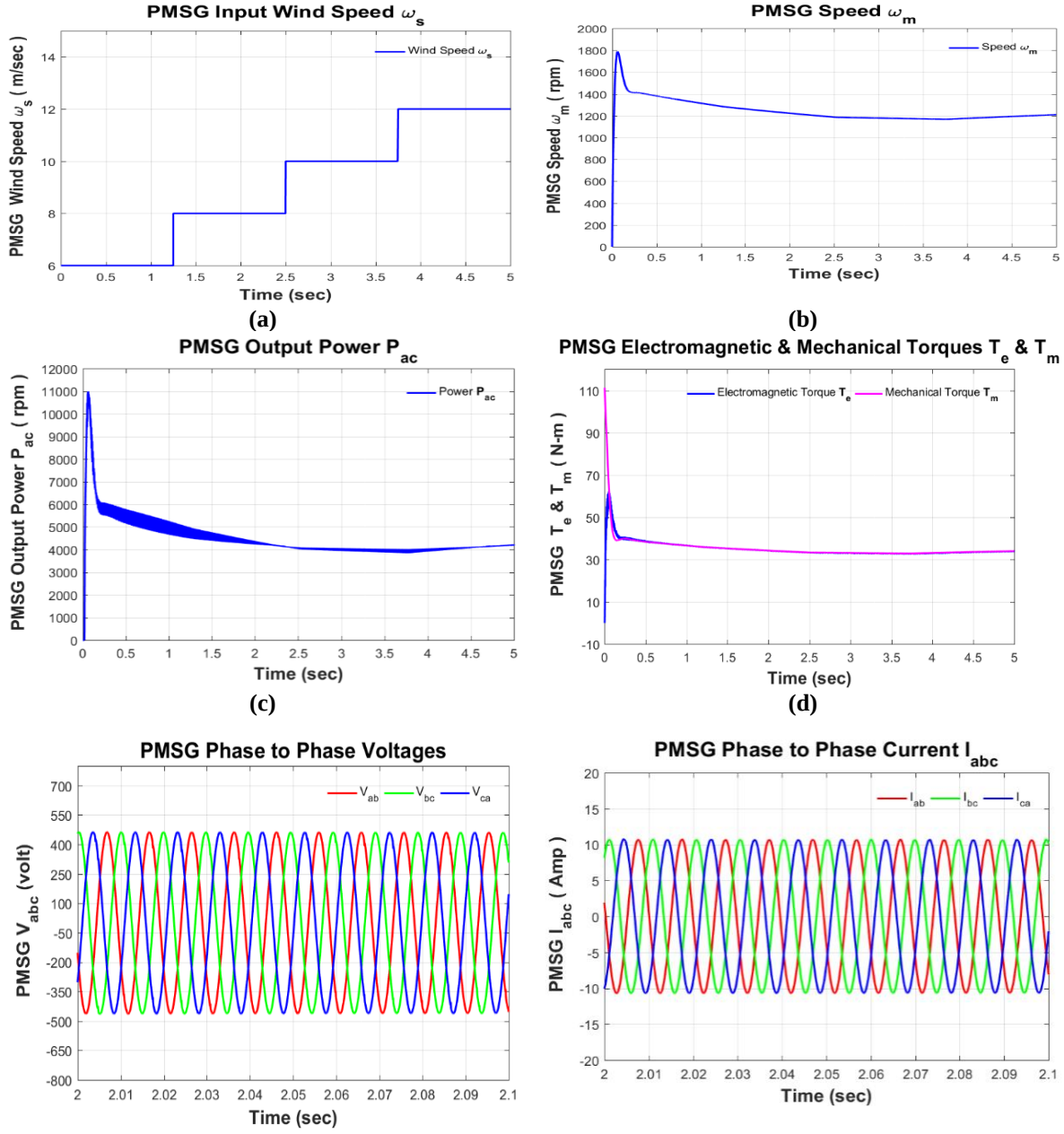

Fig. 4.1 (a) Waveform of Input Wind Speed, (b) PMSG Speed, (c) PMSG Output power, (d) Electromagnetic & Mechanical Torque, (e) PMSG Phase to Phase Voltage (f) PMSG Phase Current

Fig. 4.2 (a) and Fig. 4.2 (b) shows the waveform of PMSG d-q component of voltage V_qV_d, and PMSG d-q component of current I_qI_d.

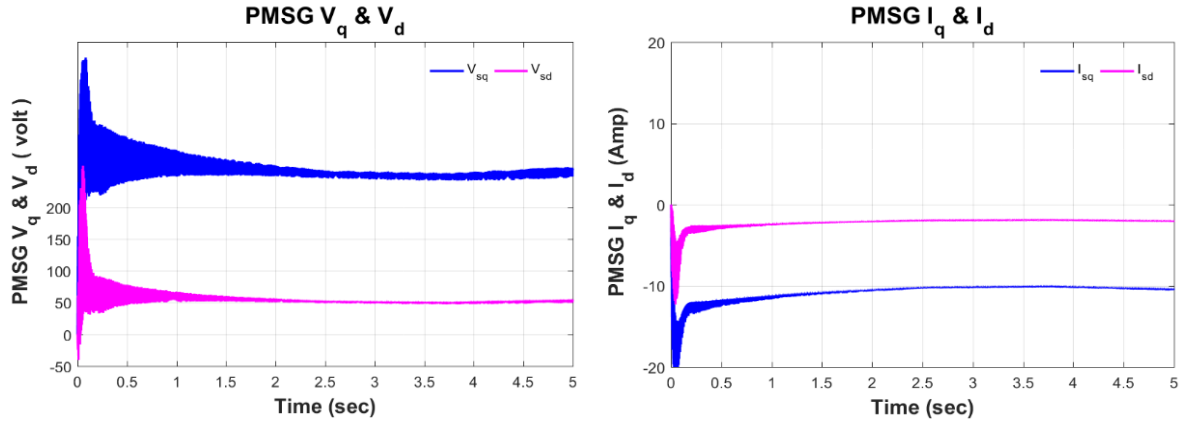

(a) **(b)**

Fig. 4.2 (a) d-q Component of Voltage V_qV_d (b) d-q component of current I_qI_d

Fig. 4.3 depicts the waveform of the DC-DC converter during the wind speed step change from 6 m/s to 8 m/s, then to 10 m/s, and finally to 12 m/s. It includes the duty ratio and the generated PWM pulses for the switch. A 5kHz PWM signal is generated in this simulation. The duty ratio value is updated every 2 milliseconds and remains constant at 0.8, as illustrated in Fig. 4.3 (a).

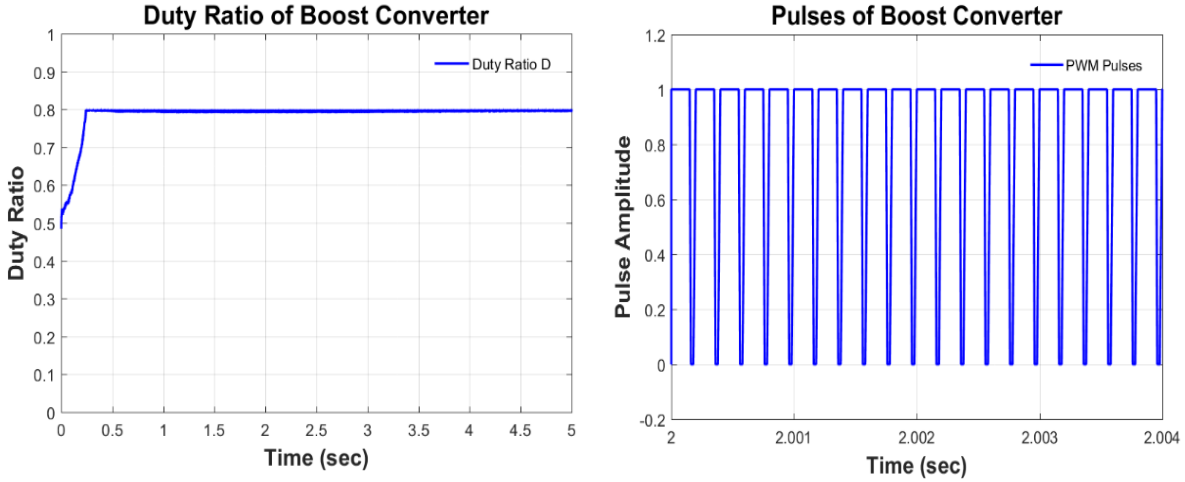

(a) **(b)**

Fig. 4.3 (a) Duty Ratio Change, (b) Pulses for DC DC Converter Switch

The DC output from the DC-DC converter is directed to DC link capacitors, which play a crucial role in maintaining a stable DC voltage at the input of the inverter. Figure 8 presents various waveforms of the multilevel inverter, including (a) multilevel inverter output voltage, (b) multilevel inverter output current, (c) multilevel inverter phase voltage, and (d) multilevel inverter duty ratio.

From the observations in Figure 8, it is evident that the multilevel inverter output current measures 45A, while the multilevel inverter output voltage remains at 500V.

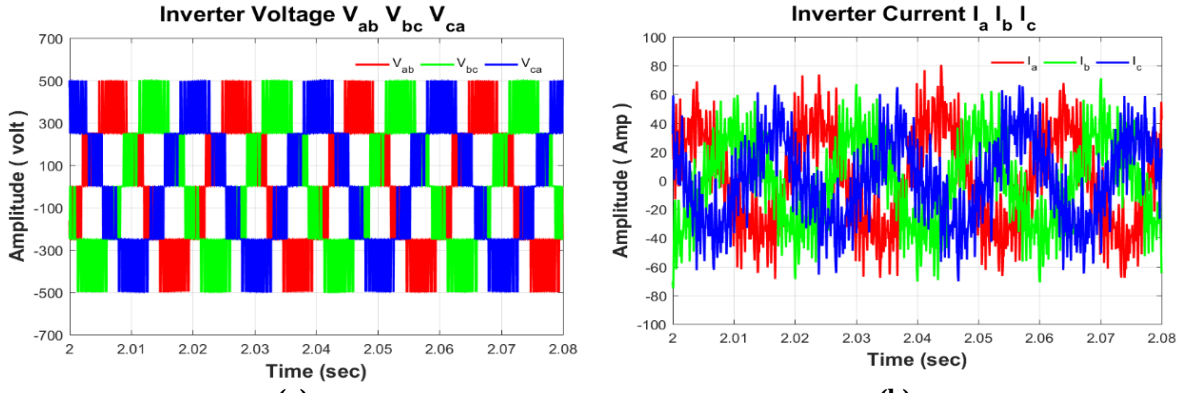

(a) **(b)**

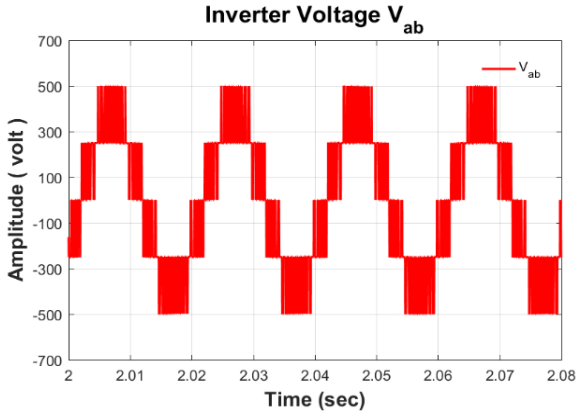

(c)

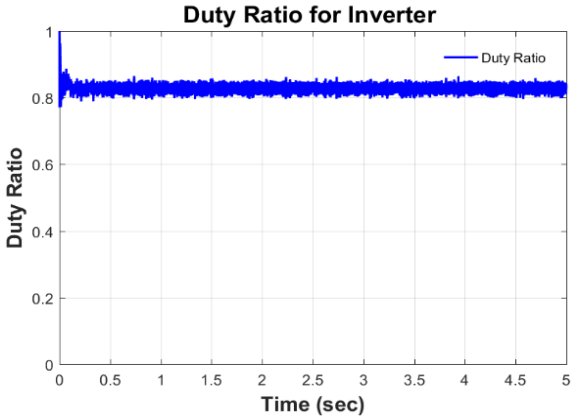

(d)

Fig. 4.4 (a) Inverter Phase to Phase Voltage, (b) Inverter Phase Current, (c) Inverter Phase to Phase Voltage (d) Duty Ration of Inverter

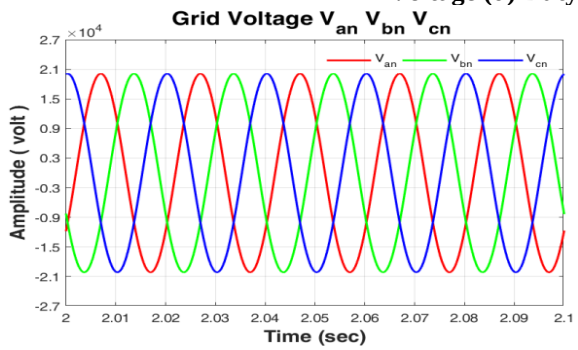

(a)

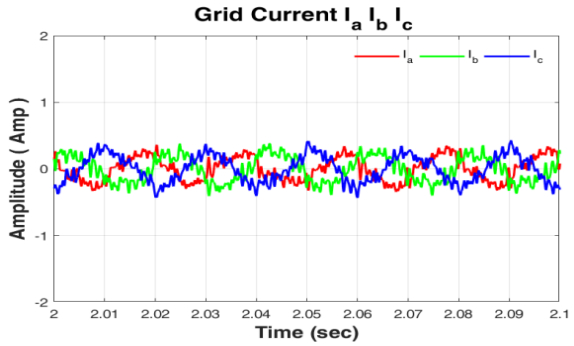

(b)

Fig. 2.9 (a) Grid Voltage, (b) Grid Current

Fig. 4.5 (a) shows the grid side phase voltages $V_{an}V_{bn}V_{cn}$. Grid voltage is maintaining at 20kV and 50Hz and Fig. 4.5 (b) shows the grid current $I_aI_bI_c$ is 0.2 p.u. So we can say from Fig. 4.5 system is stable

Case-2: Simulation results during step-changes wind speed from 12-10-8-6 m/s

In the simulation, the wind speed transitions from 12 m/s to 10 m/s, then to 8 m/s, and finally to 6 m/s for a two-drive train PMSG-based WECS, while maintaining a constant load. Fig. 4.6 illustrates the simulation results. At t=0 sec., the wind speed is 12 m/s, and at t=5 sec., it decreases to 6 m/s, with the speed remaining constant between these times. The wind speed transitions from 12 m/s to 10 m/s at t=1.3 sec., undergoes a step change from 10 m/s to 8 m/s at t=2.5 sec., and further decreases from 8 m/s to 6 m/s at t=3.8 sec. At t=5 sec., the PMSG output power is recorded at 3900W.

Fig. 4.6 illustrates that the PMSG speed decreases from 1450 rpm at t=0 to 1150 rpm at t=5 sec. Additionally, the electromagnetic torque varies from 60N-m to 32N-m, and the generated power fluctuates from 6200W to 3800W during the interval from t=0 sec to t=5 sec. The generated voltage remains regulated at 550V, and the current stays sinusoidal at 12 A, as depicted in Fig. 4.6. The waveform analysis highlights the PMSG system's superior dynamic performance in response to changing wind speeds, with noticeable improvements in torque response.

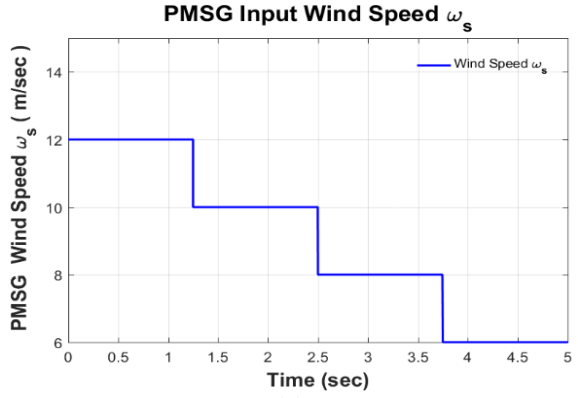

(a)

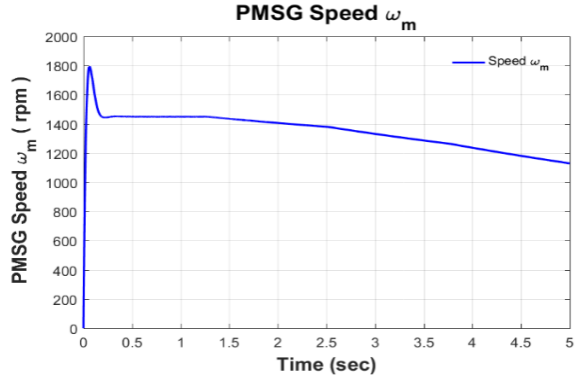

(b)

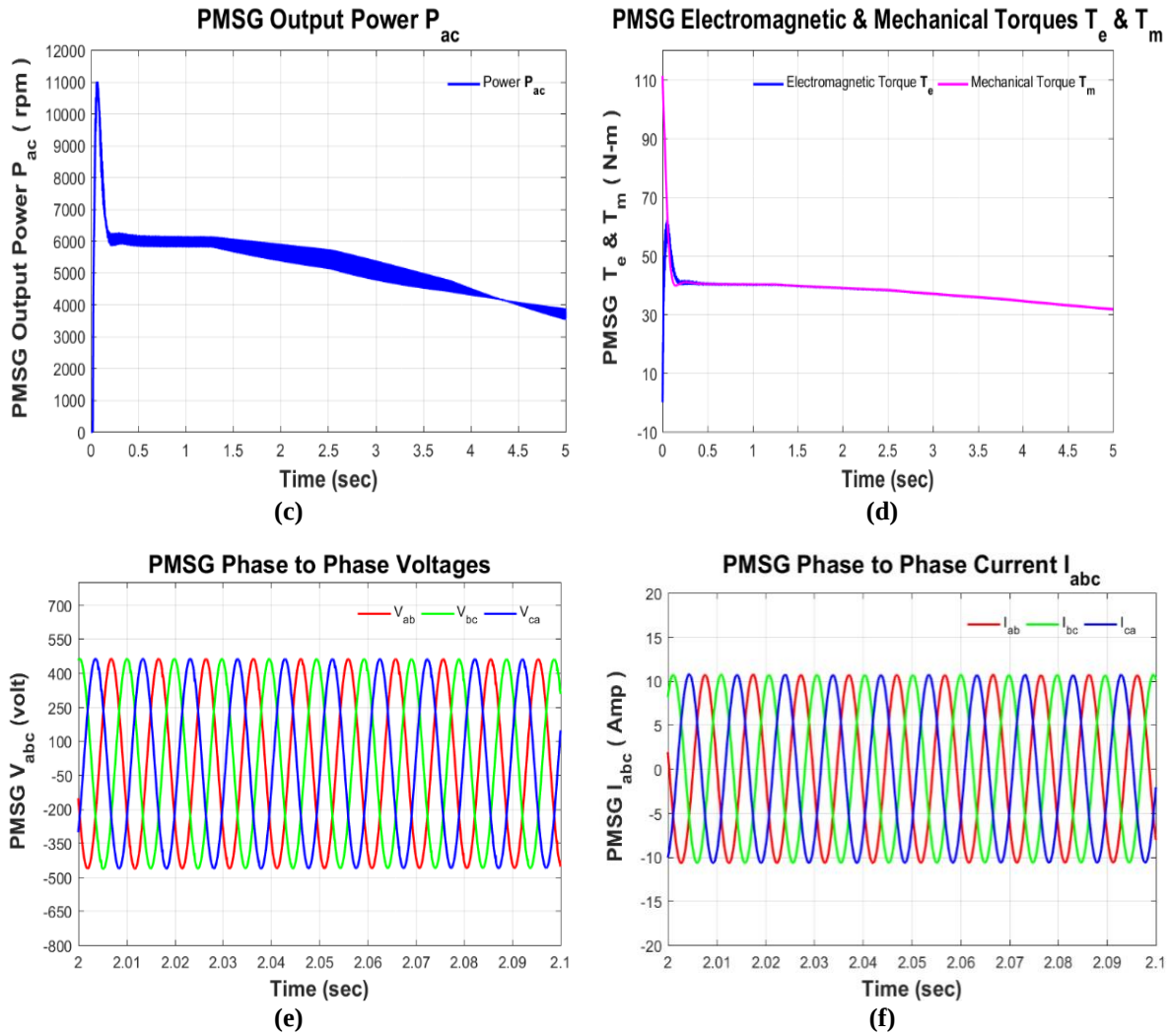

Fig. 4.7 (a) Waveform of Input Wind Speed, (b) PMSG Speed, (c) PMSG Output Power, (d) Electromagnetic & Mechanical Torque, (e) PMSG Phase to Phase Voltage (f) PMSG Phase Current

Fig. 4.7 (a) and Fig. 4.7 (b) shows the waveform of PMSG d-q component of voltage V_qV_d, and PMSG d-q component of current I_qI_d

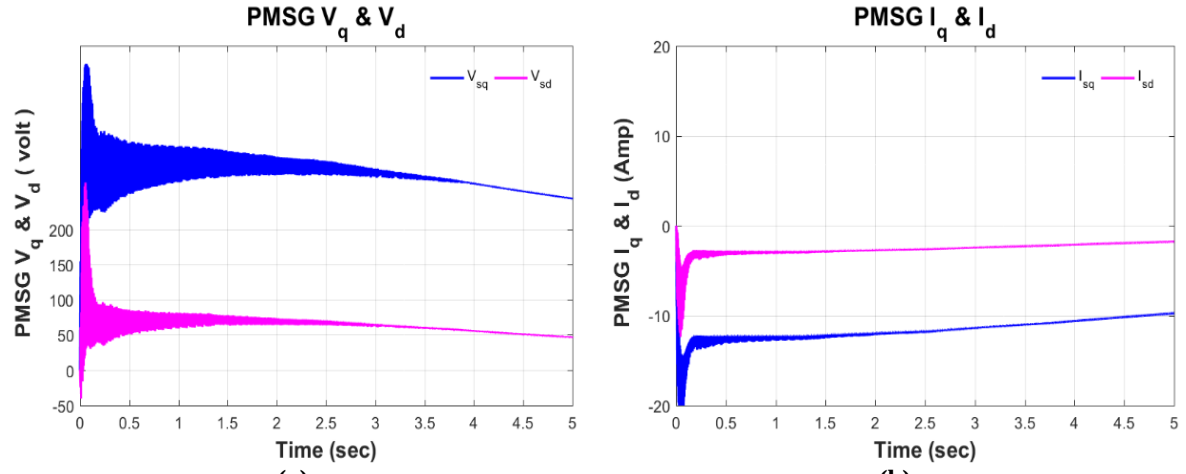

Fig. 4.8 (a) d-q component of voltage V_qV_d (b) d-q component of current I_qI_d

Fig. 4.9 illustrates the waveform of the DC-DC converter during the wind speed step change from 12 m/s to 10 m/s, then to 8 m/s, and finally to 6 m/s. It includes the duty ratio and the generated PWM pulses for the switch. A 5kHz PWM signal is generated in this simulation. The duty ratio value is updated every 2 milliseconds and remains constant at 0.8, as depicted in Fig. 4.9 (a).

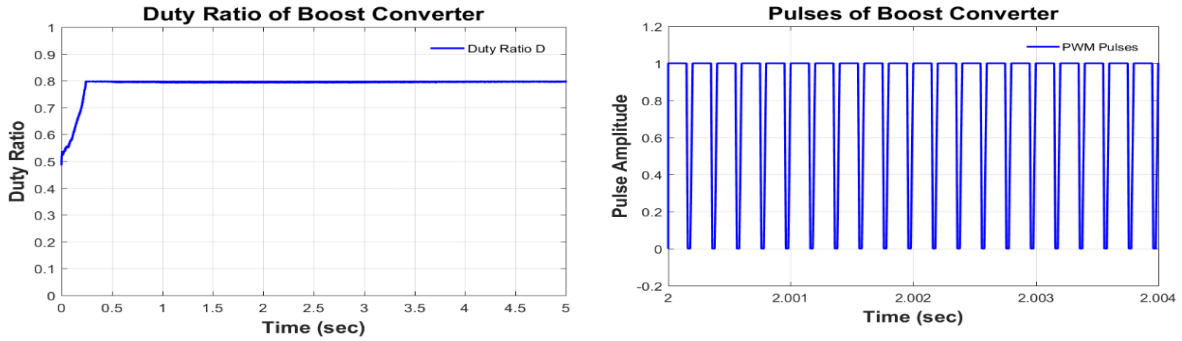

(a) (b)

Fig. 4.9 (a) Duty Ratio Change, (b) Pulses for DC DC Converter Switch

The DC output from the DC-DC converter is directed to DC link capacitors, which play a vital role in maintaining a stable DC voltage at the input of the inverter. In Fig. 4.10, various waveforms of the multilevel inverter are presented, including (a) multilevel inverter output voltage, (b) multilevel inverter output current, (c) multilevel inverter phase voltage, and (d) multilevel inverter duty ratio. Observing Figure 4.10, it is evident that the multilevel inverter output current measures 45A, while the multilevel inverter output voltage remains stable at 500V.

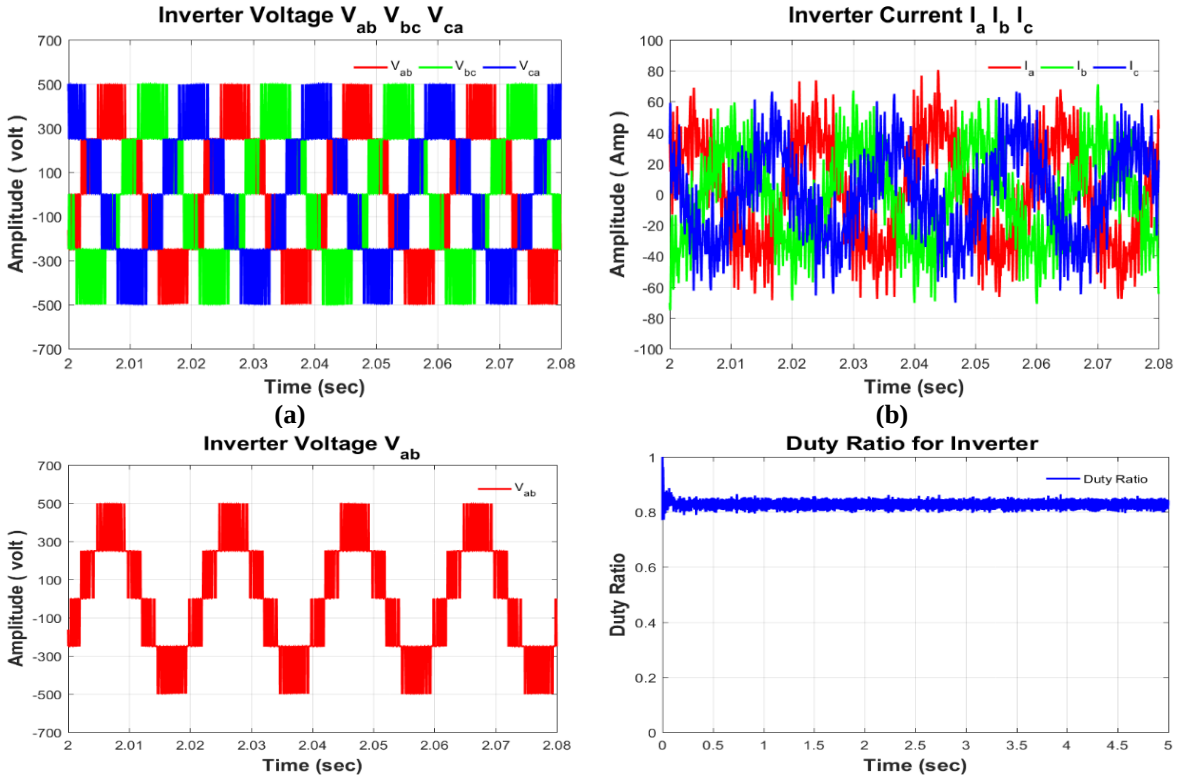

(a) (b)

(c) (d)

Fig. 4.10 (a) Inverter Phase to Phase Voltage, (b) Inverter Phase Current, (c) Inverter Phase to Phase Voltage (d) Duty Ration of Inverter

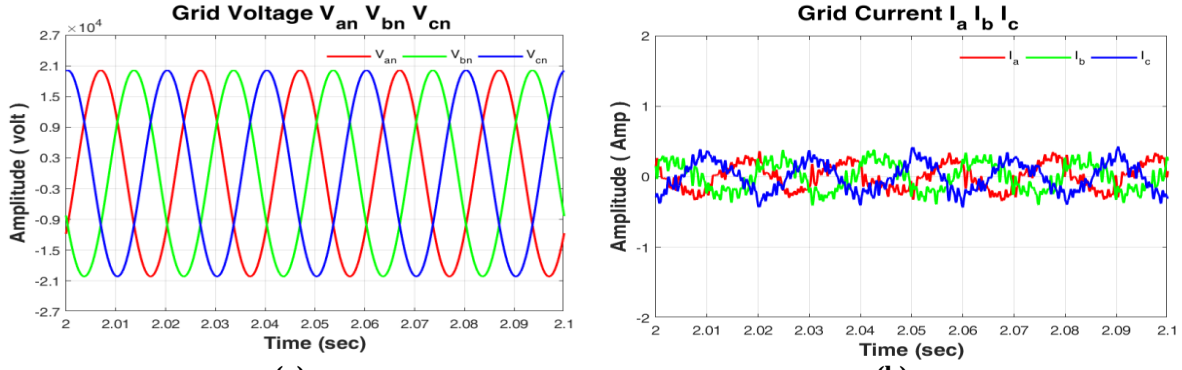

(a) (b)

Fig. 4.11 (a) Grid Voltage, (b) Grid Current

Fig. 4.11 (a) shows the grid side phase voltages $V_{an}V_{bn}V_{cn}$. Grid voltage is maintaining at 20kV and 50Hz and Fig. 4.11 (b) shows the grid current $I_aI_bI_c$ is 0.2 p.u. So we can say from Fig. 2.14 system is stable.

CONCLUSION

The controllers devised in this study underwent testing under varying wind speeds and fluctuating load conditions. Through comprehensive simulation and experimental analyses, the following conclusions were drawn: A dynamic model of the proposed PMSG-based wind generation system interfaced with a multilevel converter system was successfully formulated. The implemented control strategy showcased notable enhancements in output power and system efficiency compared to conventional methods. Simulation and experimental results demonstrated a well-balanced relationship between load voltage and load current. Moreover, the total harmonic distortion of load voltage and load current was measured at 2.67 and 1.65, respectively, for inductive loads. These values fall below 5%, aligning with the permissible limits outlined in IEEE standard-1547, IEEE-519, and IEC-61727.Consequently, the produced power meets the general standards regarding voltage and current, ensuring compliance within the 5% threshold specified by the aforementioned standards.

REFERENCES

[1] Anbarasan Palani., et. al., “A Novel Design and Development of Multilevel Inverters for Parallel Operated PMSG-Based Standalone Wind Energy Conversion Systems,” Iranian Journal of Science and Technology, Transactions of Electrical Engineering, Springer, Vol. 5, 2023.

[2] Pranupa S., et. al., “Wind energy conversion system using perturb & observe-based maximum power point approach interfaced with T-type three-level inverter connected to grid,” Clean Energy, Volume 6, Issue 4, August 2022, Pages 534–549.

[3] Feng Guo, et al., ‘‘Grid-forming control strategy for PMSG wind turbines connected to the low-frequency AC transmission system,’’ Elsevier, Energy Reports, Vol. 9, December 2023, Pages 1464-1472

[4] H. Kumawat; R. Jangid, “Performance and Investigation of Two Drive Train Interfaced Permanent Magnet Synchronous Generator for Wind Energy Conversion System”, Journal of Emerging Technologies and Innovative Research, ISSN:2349-5162, Volume 7, Issue 1, January 2020.

[5] B. Tarroja, B. Shaffer, and S. Samuelsen, ‘‘The importance of grid integration for achievable greenhouse gas emissions reductions from alternative vehicle technologies,’’ Energy, vol. 87, pp. 504–519, Jul. 2015, doi: 10.1016/j.energy.2015.05.012.

[6] M. Aarif; D. Joshi; R. Jangid and S.S. Sharma, “Grid Power Smoothing Management for Direct Drive PMSG Variable Speed Wind Energy Conversion System with Multilevel Converter”, IEEE 7th International Conference on ICT for Sustainable Development, Organized by Global Knowledge Foundation during 29-30, July 2022 at Goa, India.

[7] Y. Joshi; J.k Maherchandani; V.K Yadav; R. Jangid; S. Vyas and S.S Sharma, “Performance Improvement of Standalone Battery Integrated Hybrid System” IEEE 7th International Conference on Electrical Energy Systems (ICEES), Organized by Sri Sivasubramaniya Nadar College of Engineering during 11-13 Feb. 2021at Chennai, India.

[8] R. Jangid; J.k Maherchandani; R.R. Joshi and B.D Vairagi, “Development of Advance Energy Management Strategy for Standalone Hybrid Wind & PV System Considering Rural Application”, IEEE 2nd International Conference on Smart Systems and Inventive Technology, Organized by Francis Xavier Engineering College during November 27-29, 2019 at Tirunelveli, India.

[9] R. Jangid; K. Parikh and P. Anjana, “Reducing the Voltage Sag and Swell Problem in Distribution System Using Dynamic Voltage Restorer with PI Controller”, International Journal of Soft Computing and Engineering, ISSN: 2231-2307, Vol.-3, Issue-6, January 2014.

[10] R. Jangid; J.k Maherchandani; V.K Yadav and R.K Swami, “Energy Management of Standalone Hybrid Wind-PV System”, Journal of Intelligent Renewable Energy Systems (John Wiley & Sons, Inc.) Pages 179-198, 2022.

[11] H. Kumawat and R. Jangid, “Using AI Techniques to Improve the Power Quality of Standalone Hybrid Renewable Energy Systems”, Crafting a Sustainable Future Through Education and Sustainable Development, IGI Global, Pages 219-228, 2023.

[12] H. Kumawat; R. Jangid, “Performance and Investigation of Two Drive Train Interfaced Permanent Magnet Synchronous Generator for Wind Energy Conversion System”, Journal of Emerging Technologies and Innovative Research, ISSN:2349-5162, Volume 7, Issue 1, January 2020.

[13] R. Jangid et. al., “Smart Household Demand Response Scheduling with Renewable Energy Resources”, IEEE Third International Conference on Intelligent Computing and Control System, Organized by Vaigai College of Engineering during May 15-17, 2019 at Madurai, India.

[14] S. Kumar; R. Jangid and K. Parikh “Comparative Performance Analysis of Adaptive Neuro-Fuzzy Inference System (ANFIS) & ANN Algorithms Based MPPT Energy Harvesting in Solar PV System.” International Journal of Technical Research and Science, vol. 8, Issue 3, March 2023.

[15] S. Sharma; R. Jangid and K. Parikh "Development of Intelligent Control Strategy for Power Quality Improvement of Hybrid RES Using AI Technique" International Journal of Technical Research and Science, vol. VIII, Issue II, Feb. 2023.
[16] L. Jhala et al., "Development of Control Strategy for Power Management in Hybrid Renewable Energy System" International Journal of Technical Research and Science, vol. VI, Issue XII, Dec. 2021.
[17] Blaabjerg, F. and Ma, K. 2017. Wind Energy Systems. IEEE Transactions on Industry Applications. 105: 2116-2131.
[18] Blaabjerg, F., Liserre, M. and Ma, K. 2012.Power electronics converters for wind turbine systems. IEEE Transactions on Industry Applications. 48: 708–719.
[19] Brisset, S.,Vizireanu, D. and Brochet, P. 2008. Design and optimization of a nine-phase axial flux PM synchronous generator with concentrated winding for direct drive wind turbine. IEEE Transactions on Industry Applications. 44: 707-715.
[20] Diaz, M., Cardenas, R., Espinoza, M., Mora, A. and Wheeler, P. 2016. Modelling and Control of the Modular Multilevel Matrix Converter and its application to Wind Energy Conversion Systems. IEEE 42nd Annual Conference on Industrial Electronics Society, held at Florence, Italy during 23-26 October 2016, pp. 5052-5057.
[21] Diaz, M., Cardenas, R., Espinoza, M., Rojas, F., Mora, A., Clare, J.C. and Wheeler, P. 2017. Control of Wind Energy Conversion Systems Based on the Modular Multilevel Matrix Converter. IEEE Transactions on Industrial Electronics. 64: 8799-8810.
[22] Diaz, M., Espinoza, M., Mora, A. and Rojas, F. 2015. A Novel LVRT Control Strategy for Modular Multilevel Matrix Converter based High-Power Wind Energy Conversion Systems. IEEE 10thInternational Conference on Ecological Vehicles and Renewable Energies (EVER), held at Monte Carlo, Monaco during 31 March-2 April 2015, pp.1–11.
[23] Li, Z., Wong, S.C., Liu, X. and Huang, Y. 2015. Discrete Fourier series based Dual-Sequence Decomposition Control of Doubly-Fed Induction Generator Wind Turbine under Unbalanced Grid Conditions. Journal of Renewable and Sustainable Energy. 7: 123-130.
[24] Liserre, M., Sauter, T. and Hung, J.Y. 2010. Future Energy Systems: Integrating Renewable Energy Sources into the Smart Power Grid through Industrial Electronics. IEEE Industrial Electronics Magazine. 4: 18–37.
[25] Long, T., Shao, S., Malliband, P, Abdi, E. and McMahon, R.A. 2013. Crowbar Less Fault Ride through of the Brushless Doubly Fed Induction Generator in a Wind Turbine under Symmetrical Voltage Dips. Transactions on Industrial Electronics. 60: 2833-2841.
[26] Lopez, J., Gubia, E., Olea, E., Ruiz, J. and Marroyo, L. 2009. Ride Through of Wind Turbines with Doubly Fed Induction Generator under Symmetrical Voltage Dips. IEEE Transactions on Industrial Electronics. 56: 4246-4254.
[27] Makrini, A.El., Karkri, Y.El., Boukhriss, Y., Elmarkhi, H. and Moussaoui, H.E. 2017. LVRT Control Strategy of DFIG based Wind Turbines Combining Passive and Active Protection. International Journal of Renewable Energy Research. 7: 1258-1269.